Heliyon 11 (2025) e41990

Contents lists available at ScienceDirect

Heliyon

journal homepage: www.cell.com/heliyon

Research article

Quantification of external disturbance forces in sliding microwire

Fazlar Rahman [a,b,*], M.A. Salam Akanda [a]

[a] Department of Mechanical Engineering, Bangladesh University of Engineering and Technology (BUET), Dhaka, Bangladesh
[b] Department of Mechanical and Production Engineering, Ahsanullah University of Science and Technology (AUST), Dhaka, Bangladesh

ARTICLE INFO

Keywords:
Microwire
MEMS devices
Disturbance force
Adhesive force
Surface force
Contact force

ABSTRACT

Due to microscale size and infinitesimal stiffness, the undesirable surface and external forces influence the mechanical behaviors of microstructures. It hinders MEMS functions, degrades reliability, and acts as a disturbance. Since MEMS functions based on microstructure mechanical behaviors, therefore, their quantification in microstructures is vital. However, the direct quantification is costly, difficult, and requires a controlled environment and unique experimental setups. Analytical assessment is also complex because of multi-physics involvement, nonlinearity of forces, and a lack of suitable mathematical models. Numerical analysis of microstructures is performed in the absence of all disturbance forces, whereas their influences cannot be eliminated during the experiment. This study aims to quantify the sum of disturbance forces in a microwire for the push-pull sliding motion against two opposite microprobes from the difference between experimental and numerical study and incorporating adhesive and electrostatic forces from literature for a single microprobe. The effect of the nonlinearity of surface forces is counted by iterating the initial difference of forces for which the numerically predicted contact force matches the experimental one. The sum of surface and external disturbance forces in the microwire is estimated to be 0.295 μN, including external disturbances of 0.177 μN. The predicted adhesive, electrostatic, and the sum of van der Waals, capillary, and hydrogen bonding forces are 0.118034, 0.02014, and 0.097894 μN, respectively. This study will help in quantifying disturbance forces in microstructures, like microbars, microrods, microplates, etc., and the appropriate design of MEMS devices.

1. Introduction

MEMS devices, whose sizes range from 1 to 100 μm, are widely employed in the robotics, electronics, communication, defense, and automotive industries, among other areas [1]. Miniature-scaled MEMS sensors are also used in the medical field to monitor brain activity, respiratory organs, developing drugs, blood vessels, vital sign detection [2], and robotic surgery [3,4]. Besides, some microstructures, such as micro-cantilevers, are used to manipulate micro-objects, embryos, tissues, and biological cells in medical research [5]. Furthermore, MEMS inertia sensors, such as inertial measurement units (IMU), accelerometers, and gyroscopes, are used in UAVs and airplanes for fault diagnosis (FD) and detection and improving reliability [6,7]. Therefore, reliability, precise and on-time response, and fatigue life of MEMS sensors and microstructures are vital for their application in medical and other crucial fields. Microstructures, such as wires, bars, spheres, membranes, beams, gears, springs, channels, rollers, spirals, coils, diaphragms, plates,

* Corresponding author. Department of Mechanical Engineering, Bangladesh University of Engineering and Technology (BUET), Dhaka, Bangladesh.
E-mail address: fazlar.rahman.mpe@aust.edu (F. Rahman).

https://doi.org/10.1016/j.heliyon.2025.e41990
Received 11 April 2024; Received in revised form 14 January 2025; Accepted 15 January 2025
Available online 15 January 2025

etc., are used in MEMS sensors [8–13]. For sensing and actuating, at least one mechanical characteristic of microstructures, such as deformation, twisting, deflection, rotation, sliding motion, carrying loads, etc., is employed in MEMS sensors [5,8,11,14]. Hence, the appropriate mechanical behavior of microstructures is essential for the precise function and endurance of MEMS sensors. However, microstructures have high aspect and surface-to-volume ratios [15,16], miniscule size [17], and infinitesimal mechanical stiffness [18]. As a result, various surface forces, such as van der Waals, electrostatic, hydrogen bonding, Casimir forces, covalent bonds, dipole-dipole interactions, capillary condensation, asperity nano-welding, etc. [5], impact the microstructure's mechanical [19,20] and micro-contact behaviors [11,21]. Therefore, these surface forces act as hinders or disturbances of MEMS function and reliability. When a microstructure touches another one, the surface forces, external disturbances, and applied mechanical force or field interplay at contact surfaces [22,23]. As a result, they cannot detach because of their infinitesimal mechanical stiffness [15,24], even in the absence of externally applied force or field. If the sum of the surface forces and external disturbance exceeds the elastic restoring force, microstructures also adhere together [15,18], and it leads to stiction and dysfunction of MEMS devices [23,25]. Primarily, electrostatic, hydrogen bonding, capillary, and van der Waals forces cause adhesion in microstructures [23,24,26], which affect microstructure contact behavior and promote stiction. Besides, dipole-dipole interactions, covalent bonds, Casimir forces, capillary condensation, and asperity nano-welding [23], if any, play roles in adhesion [18,27,28]. However, their effect is insignificant and negligible.

MEMS sensors function based on the Lorentz force, which is developed from the interaction of electric current and magnetic fields [29]. One or more fields, such as electrostatic, piezoelectric effect, thermal load or gradient, and electric and magnetic fields, are used to actuate MEMS sensors [24,30]. Therefore, due to the Eddy current, Hall, and Seebeck effects, a third field or force develops [31] within microstructures or MEMS sensors in the presence of any one of these fields, such as temperature gradient (∇T), magnetic field (B), and electric field (E) [32]. This third force or field acts as a hindrance and interferes with the microstructure's mechanical behavior. It affects the response and reliability of MEMS sensors, even if only one force or field is used for actuating or sensing. The remaining or undesirable forces work as disturbances of MEMS sensors. For example, if a microstructure is exposed to a temperature gradient (∇T) and a magnetic field (B) concurrently at right angles, an electric field (E) will develop in the third direction [33]. To evaluate the microstructure behavior, reliability, and response of MEMS sensors precisely, the prediction of disturbance forces is vital. Without identifying, controlling, and quantifying disturbance forces, the appropriate design of MEMS sensors and manipulation of micro-objects, such as biological cells, tissues, embryos, etc., cannot be achieved. This study aims to quantify the disturbance forces arising from external sources or fields in a microwire for push-pull sliding motion against two opposite microprobes.

MEMS technology is a fascinating topic among researchers and has grown rapidly [34,35]. However, due to the micro-scaled size, heterogeneity, and non-linearity of surface forces, there is a lack of suitable analytical methods and techniques to quantify disturbance forces in microstructures [19,36]. Besides, MEMS sensors and components are diverse and have broad applications and functions [36,37]. It is challenging to associate and quantify disturbance forces in microstructures [38] and requires multi-disciplinary skills to comprehend [34,36,37]. Furthermore, the intricacy of surface physicochemical processes [19,39], tribological effects at micro-scales [22,28,40], non-standard boundary conditions, non-linearity, electro-mechanical coupling, heterogeneous integration, and non-homogeneity [36,38] intricate the mathematical modeling and analytical technique [19] to quantify disturbance forces in microstructures. Therefore, the analytical assessment is complex because of multi-physics involvement and a lack of suitable mathematical models. In contrast, the direct quantification of disturbance forces in microstructures is also complicated since it requires a controlled environment, unique and costly experimental setups, as well as remarkable skills and efforts due to their minuscule size. However, numerical analysis of microstructure is performed in the absence of all disturbance forces, whereas their influences cannot be eliminated during the experimental study. Therefore, the sum of all disturbance forces in the microstructure can be quantified indirectly from the difference between experimental and numerically evaluated contact forces under the identical scenario. This novel perception is exploited in this study to assess the disturbance forces in a microwire for push-pull sliding motion against two opposite microprobes without using force sensors.

Some studies have reported suppression, rejection, and control of disturbance forces in microstructures. Deng et al. [41] examined the disturbance suppression in MEMS inertia sensors. Dong and Edwards [42] investigated the disturbance rejection of electrostatically actuated MEMS sensors. Liu et al. [43] examined the static and dynamic instability of the MEMS cantilever system exposed to weak and robust disturbances. Zheng et al. [44] studied the disturbance rejection control in MEMS gyroscopes. Qiao et al. [45] investigated the reliability of electrostatically actuated MEMS resonators exposed to random mass disturbances. Rahman and Akanda [32] investigated minimizing surface driving and disturbance forces in microstructures. Still, there is a shortfall of studies regarding quantifying disturbance forces in microstructures. In this study, the sum of disturbance forces in a sliding microwire is quantified indirectly for sliding motion against two opposite microprobes by comparing the numerical analysis with the experimental study. The methodology presented in this study can be used to compute disturbance forces in other microstructures, such as microplates, microrods, microbars, etc. It will aid in designing MEMS sensors and manipulating micro-objects with higher accuracy and reliability.

2. Methodology

2.1. Geometry and micro-contact arrangement

The analytical assessment of disturbance force in microstructures is complex due to the lack of suitable mathematical models [36,38]. Experimental quantification is also difficult and costly. Besides, due to the ambiguity of the type and initiation time of external fields or forces, the analytical prediction becomes more complex. Numerical investigations are performed without the presence of disturbance forces. Therefore, the sum of all disturbance forces in the microstructure can be predicted indirectly by comparing the

experimental and numerically evaluated contact or surface forces. The micro-contact arrangement, as shown in Fig. 1, is used in this study to quantify the sum of all disturbance forces in a microwire. The micro-contact arrangement includes a platinum microwire, two tungsten microprobes, and a Double Beam Cantilever (DBC), which is kept identical to the available experimental study [11].

The platinum microwire of 65 μm length and 0.625 μm diameter is supported between two opposite tungsten microprobes of 5.0 μm diameter by frictional contacts, as shown in Fig. 1. One end of the microwire is bonded to the tip of the Double Beam Cantilever (DBC) by joule heating. The DBC is used to manipulate the microwire along the longitudinal direction by applying displacement at the end 'B' of the DBC, which developed push and pull sliding motions to the microwire due to the stiffness of the DBC. It is made of structural steel. The length and stiffness of the DBC are 22.75 μm and 1.10 μN/μm, respectively. The distance between microprobes is 10 μm, and the length of the microwire extended portion is 5.0 μm.

2.2. Analysis strategy

The contact force between tungsten microprobes and the platinum microwire is 0.8217 μN, which is evaluated experimentally by Akanda et al. [11] for the pull-push sliding motion of the microwire and using the identical arrangement of Fig. 1. In the study of Rahman and Akanda [1], the contact force at both microprobes is quantified numerically for the same scenario, load, boundary conditions, and material of the experimental study [11]. It is found to be 0.5713 μN by taking the sum of tangential contact forces at two microprobes. The experimental [11] and numerically [1] evaluated contact forces in the microwire are shown in Fig. 2.

The difference in contact force between the experimental observation [11] and numerical study [1] is found to be 0.25037 μN, which is considered an apparent reference of the sum of all disturbance forces acting from surface and external fields or forces to the microwire. The effect of the nonlinearity of contact forces is incorporated by varying the initial difference of forces through iteration until the numerically evaluated contact force matches the experimental one. The microwire's external disturbance forces are quantified by synthesizing the results of this investigation as well as available experimental [11] and numerical studies [1,23].

2.3. Numerical modeling

The identical configuration of platinum microwire, microprobes, and Double Beam Cantilever (DBC), as shown in Fig. 3 [1], is modeled in the numerical analysis tool ANSYS Workbench. An additional force, 'F', is applied at the right end of the microwire and in the opposite direction of the sliding motion, which represents the sum of all disturbance forces in the microwire. Though disturbance force acts over the entire surface of the microwire in real situations, in this study, it is applied at the free end of the microwire for suitable convergence of the FEA.

In numerical analysis, the farthest microprobe is constrained as a fixed support and referred to as a 'Fixed Probe'. Another one, referred to as a 'Load Probe', is displaced only along the lateral direction of the microwire [1]. The end 'B' of the DBC is only able to move along the axial direction of the microwire [1]. Displacement applied at the end 'B' of the DBC will develop axial force in the microwire and generate push-pull sliding motion in the microwire against two opposite microprobes, where it experienced resistive friction force. Since it is a contact problem, the solution of the nonlinear contact problem is achieved by solving the following nonlinear governing equation using the numerical analysis tool ANSYS Workbench [46].

$$\{F\} = [K(\{U\}) + S(\{U\}) - S'(\{U\})]\{U\}$$

where, [K] = Global stiffness matrix, {U} = Displacement vector, and {F} = Input force vector, S = Stress stiffening matrix, and S' = Spin softening matrix.

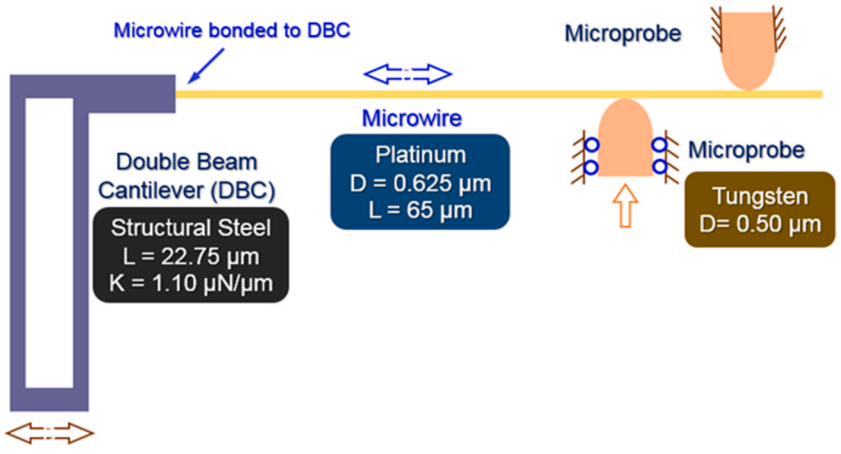

Fig. 1. Micro-contact arrangement of microwire, microprobes, and DBC.

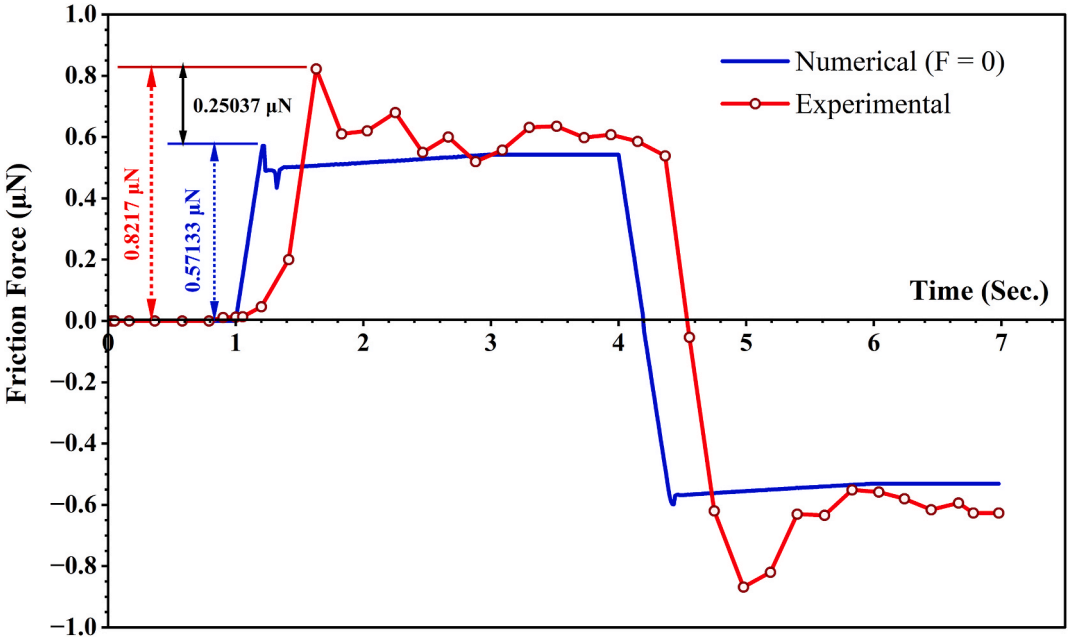

Fig. 2. Difference between experimental and numerically evaluated contact forces.

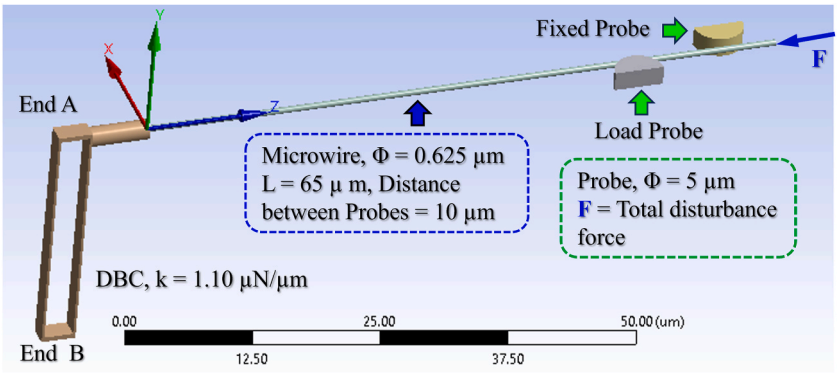

Fig. 3. Geometric configuration used in numerical analysis [1].

2.4. Boundary conditions

In this study, boundary conditions, load, meshing, time steps of the analysis, and sliding velocity of the microwire are kept the same as in the numerical analysis available in the study of Rahman and Akanda [1]. The boundary conditions employed in this study are depicted in Fig. 4 from the reader's point of view. The corresponding displacement of the Load Probe, end 'B' of the Double Beam Cantilever (DBC), and the direction of the external force 'F' are shown in Table 1. The force 'F' is applied at the right end of the microwire and opposite to its axial motion (Fig. 4). The end 'B' of the DBC is only allowed to be displaced along the longitudinal direction (along Z-axis) and the Load Probe only along the lateral direction (along X-axis) of the microwire [1]. The Fixed Probe is constrained as a fixed support (Fig. 4) [1].

Material properties and geometry are also retained, identical to the available experimental [11] and numerical [1] studies. The displacement applied at the end 'B' of the DBC and Load Probe, the magnitude and direction of disturbance forces 'F', which is varied gradually in the iteration, are shown in Fig. 5.

The displacement of 1.101 μm is applied to the Load Probe along the lateral direction of the microwire from 0 to 0.75 s, and it remains in the displaced position during the whole time period (Table 1). Then, the displacement of 5.0 μm is employed at the end 'B' of the DBC from 1.0 to 3.0 s (V = 2.5 μm/s) while pushing forward motion of the microwire, and it is pulling backwards to the initial position form from 4.0 to 6.0 s (V = 2.5 μm/s) [1], as shown in Fig. 5(a) and Table 1. During the pushing forward and pulling backwards of the microwire, the total disturbance force 'F' is applied at the end of the microwire and in the opposite direction of the sliding motion, as shown in Fig. 5(b) and Table 1. It is varied from the initial or reference value of F = 0.25037 μN until the numerically

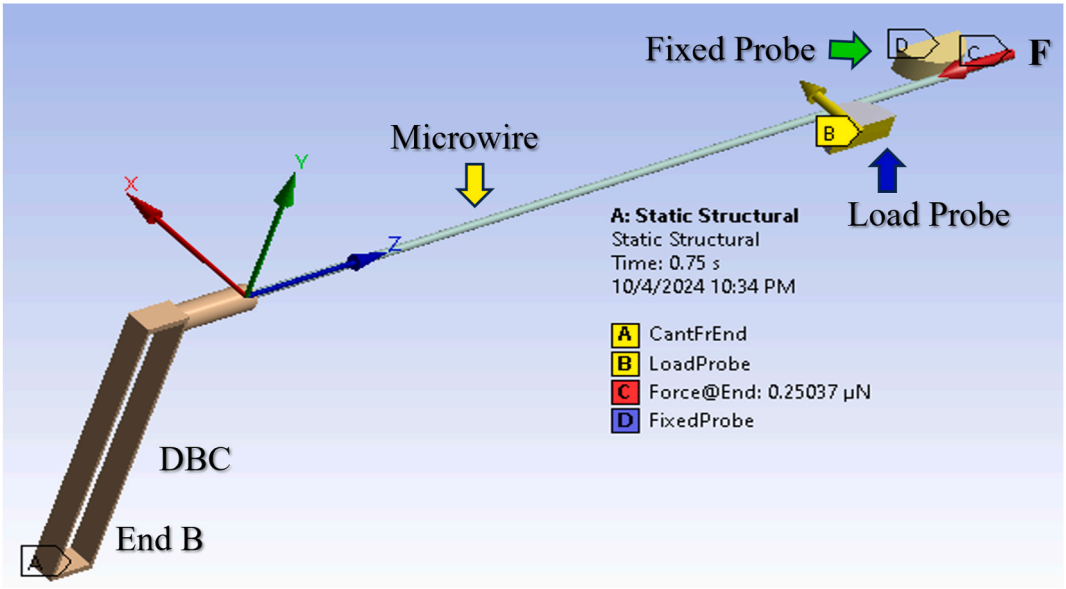

Fig. 4. Boundary conditions [1] and external disturbance force 'F'.

Table 1
Displacement of Load Probe, End B of DBC, and direction of force 'F'.

Steps No.	Time (s) (0–6.98 s)	Load Probe Disp. (X, Y, Z)	Fix Probe Disp. (X, Y, Z)	End B (DBC) Disp. (X, Y, Z)	F (μN) (X, Y, Z)
1	0–0.75 s	(1.101 μm, 0, 0)	(0, 0, 0)	(0, 0, 0)	(0, 0, -F)
2	0.75–1.0 s	(1.101 μm, 0, 0)	(0, 0, 0)	(0, 0, 0)	(0, 0, -F)
3	1.0–3.0 s	(1.101 μm, 0, 0)	(0, 0, 0)	(0, 0, 5.0 μm)	(0, 0, -F)
4	3.0–4.0 s	(1.101 μm, 0, 0)	(0, 0, 0)	(0, 0, 5.0 μm)	(0, 0, F)
5	4.0–6.0 s	(1.101 μm, 0, 0)	(0, 0, 0)	(0, 0, 0)	(0, 0, F)
6	6.0–6.98 s	(1.101 μm, 0, 0)	(0, 0, 0)	(0, 0, 0)	(0, 0, F)

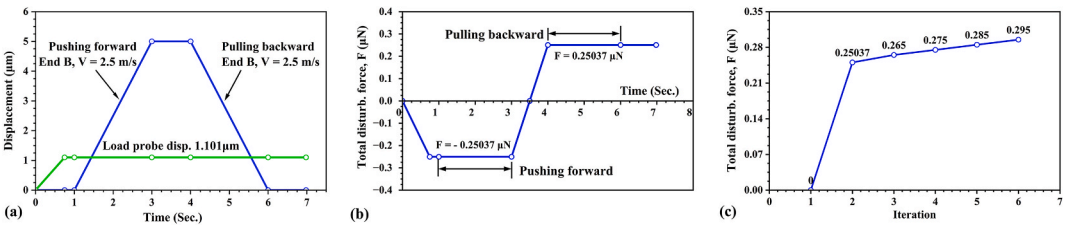

Fig. 5. (a) Displacement applied at the end 'B' of the DBC and Load Probe [1,11], (b) Direction of 'F' during sliding motion of microwire, and (c) Magnitude of 'F' varied to match numerically predicted contact force to the available experimental study.

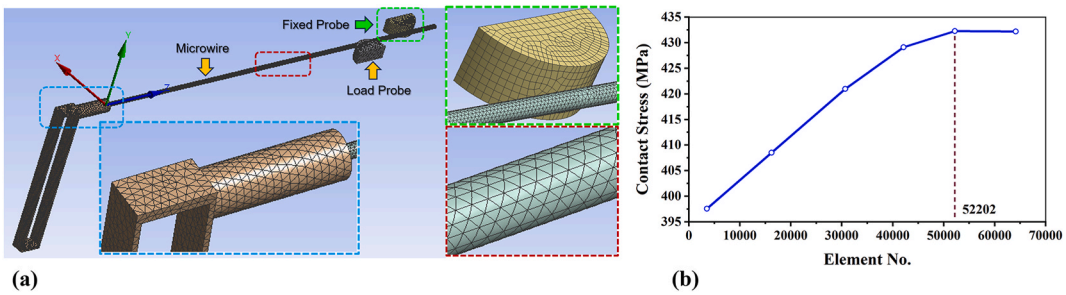

Fig. 6. (a) Meshing of Microwire, DBC and Probes, and (b) Mesh convergence [1].

evaluated contact force becomes equal to the experimentally evaluated contact force of 0.8217 μN [11], as shown in Fig. 5(c).

2.5. Meshing

Solution time, convergence, and precision of the numerical analysis stand on the element type and mesh density. In this study, the double beam cantilever (DBC), microprobes, and microwire are meshed using higher-order solid elements as per the study of Rahman and Akanda [1]. The 52202 elements employed in the meshing include hexahedrons, tetrahedral, pyramid, and wedge elements, as shown in Fig. 6(a). The contact surfaces are meshed with CONTA 175, CONTA 174, and TARGE 170 contact elements. The mesh convergence is accomplished through variation of the number of elements over maximum contact stress in the microwire, as shown in Fig. 6(b). It is achieved by reducing the element size or increasing the element number in the model successively until the maximum contact stress in the microwire becomes independent of the mesh density [1]. The maximum contact stress in the microwire becomes almost constant between element numbers 52,202 and 64,115 (Fig. 6(b)). However, this study uses the model with 52,202 element numbers to reduce the run time.

2.6. Setting of nonlinear analysis

This study uses the FEA tool ANSYS Workbench to solve the contact analysis between the microwire and microprobes. It evaluates the contact force in the microwire for push-pull sliding motion against two microprobes. The contact behavior of microstructure is erratic, unanticipated, and challenging to solve [47]. Furthermore, contact analysis is extremely nonlinear and difficult to converge [1, 48]. The contact bodies may be pierced or detached from one another without distributing loads and converging the solution, which depends on the load, boundary conditions, surface, and contact type, as well as time steps and sub-steps [23]. For convenient convergence of nonlinear contact problems, each time step is split into a number of sub-steps for applying load gradually, and the whole loading period is split into a number of time steps [1,49]. In this study, the whole loading period, 0–6.98 s, is split into six-time steps (Table 1), and each time step is split into 340 initial, 210 minimum, and 680 maximum sub-steps according to the numerical study of Rahman and Akanda [1]. To accelerate the convergence of the contact solution, the direct or sparse solver is used with the large deflection option kept on.

3. Results and discussion

This study aims to predict the external and surface disturbance forces in the microwire for push-pull sliding motion against two opposite microprobes. Quantifying disturbance forces in microstructures is vital to ensuring MEMS's reliability, fatigue life, and suitable functionality. Since it works based on the mechanical behavior of the microstructure. However, their analytical evaluation is difficult due to the lack of suitable mathematical models, and experimental evaluation is also costly due to its tiny size and nonlinearity of forces. Since it requires distinct skills and expensive and unique experimental setups. Hence, this study synthesizes available

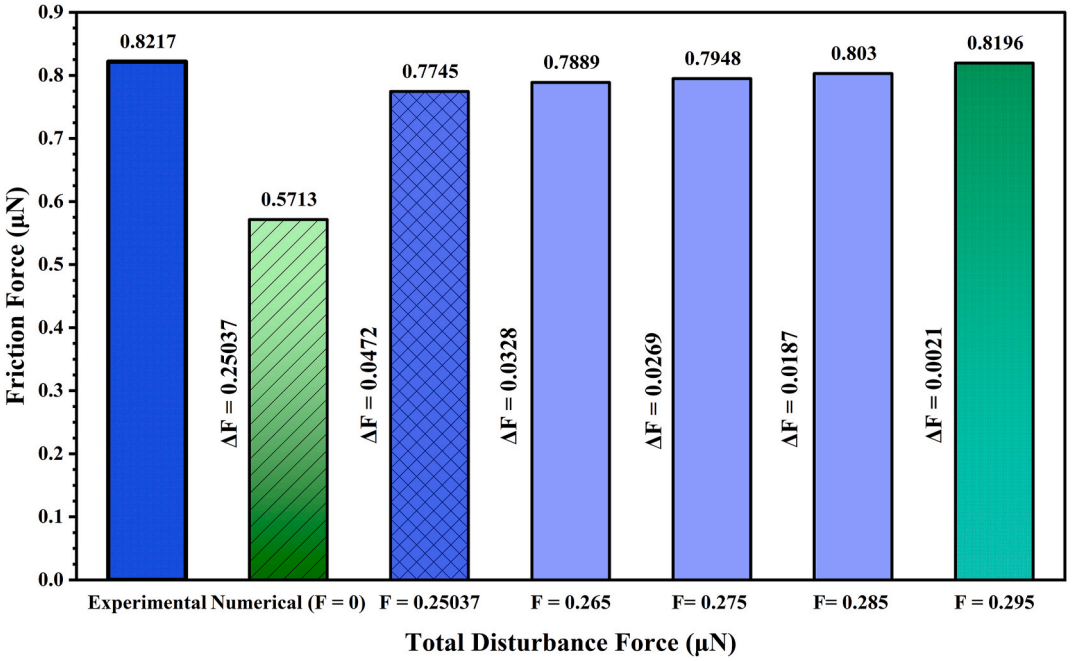

Fig. 7. Sum of all disturbance forces 'F' in the microwire evaluated by numerical analysis.

experimental [11] and numerical studies [1] to assess the external and surface disturbances in the microwire without using force sensors or experimental setups. Besides, the nonlinearity of disturbances is also incorporated in the analysis by iterations. The result is validated by comparing the contact force and stick-slip behavior with the available experimental study [11], as well as by investigating the acceptable deformation and contact behavior of the microwire. It is a novel method and can be used to quantify disturbance forces in other sliding microstructures, such as microplates, microrods, microbars, etc.

3.1. Quantification of total disturbance force

The magnitude of total disturbance forces 'F' is varied from 0.25037 μN by 0.10 μN increment in the numerical analysis, as shown in Fig. 7, until the magnitude of contact force in the microwire becomes very close or equal to the experimental contact force of 0.8217 μN [11]. The magnitude of contact force and corresponding contact behavior of the microwire are shown in Figs. 7 and 8, respectively.

The pattern of the contact behavior curves of the microwire for the variation disturbance force 'F' (shown in Fig. 8) is found to be similar to the experimental study [11] as well as to the numerical study [1]. The sum of all disturbance forces in the microwire is predicted as F = 0.295 μN by numerical analysis, for which the contact force is predicted as 0.8196 μN, since it becomes very close to the experimental contact force of 0.8217 μN [11] (Figs. 7 and 8). The difference of contact forces is ΔF = 0.0021 μN, and 99.74 % precision is achieved in the numerical analysis with respect to the experimental prediction. The error or uncertainty of the numerical analysis is only 0.26 %, which shows very good agreement between experimental and numerical studies. For 'F = 0', the difference between the experimental and numerically predicted contact force is 0.25037 μN. Due to the non-linearity, the sum of all disturbance forces is quantified to 0.295 μN, which is increased by 0.04463 μN (17.43 %) from the reference or apparent sum of disturbance forces (0.25037 μN). It justifies the accomplishment of the numerical analysis since surface forces arising from external sources/fields and contact behavior are nonlinear. The maximum contact pressure in the microwire and at the location of the Load Probe is found to be 434.43 MPa for the sum of all disturbance forces or total disturbances, $F_D = 0.295$ μN, as shown in Fig. 9. It is found to be lower than the yield strength of the platinum microwire ($\sigma_y = 630$ MPa [11]), which specifies the suitability of this study.

Total disturbance force, $F_D = 0.297$ μN, which is 51.64 % of the externally applied or numerically evaluated contact force (0.5713 μN) and 36.14 % of the experimentally predicted contact force (0.8217 μN). Therefore, the effect of disturbance forces in the microstructure cannot be discarded for proper functions of MEMS and microstructures, and its quantification is essential.

3.2. Quantification of external disturbance force

The disturbance force active on the microwire from external sources or fields is quantified by the synthesized results of the current study and numerical studies available in the literature [1,23]. The electrostatic and adhesive forces are assessed as 0.059017 μN and 0.01007 μN, respectively, for the single contact between the microprobe and microwire by Rahman and Akanda [23]. In this study, the microwire slides across two microprobes and maintains contact during the push-pull sliding motion. Therefore, the adhesive and electrostatic forces in the microwire will be double those of the single contact.

For double contacts,

$$F_{Elec} = 0.01007 \times 2 = 0.02014\ \mu N$$

$$F_{Adhe} = 0.059017 \times 2 = 0.118034\ \mu N$$

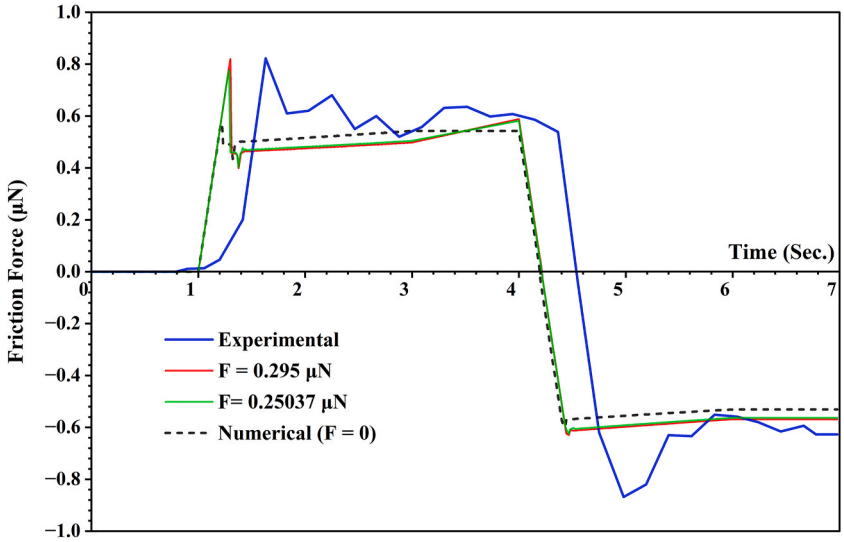

Fig. 8. Magnitude of contact force and contact behavior of the microwire for variations of sum of all disturbance forces 'F'.

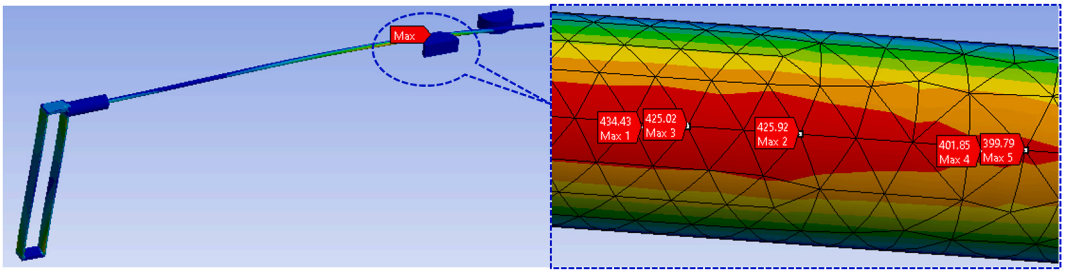

Fig. 9. Location and magnitude of maximum contact pressure in the microwire.

Where, F_{Elec} and F_{Adhe} denote the electrostatic and adhesive force in the microwire, respectively.

The sum of all disturbance forces, or total disturbance forces, in the microwire for double contact $F_D = 0.295\ \mu N$ (Figs. 6 and 7), which arises from the external disturbances and also from the surface forces, such as adhesion [15,36]. Therefore, the sum of the disturbance forces arising from all external sources or fields can be determined from the following relationship [15,36].

$$F_D = F_{Adhe} + F_{Ex\_distb}$$

$$F_{E\_distb} = F_D - F_{Adhe} = (0.295 - 0.118)\ \mu N = 0.177\ \mu N$$

where, F_{E_distb} is the external disturbance active in the microwire.

In addition, van der Waals, electrostatic, capillary, and hydrogen bonding are the leading contributors to the adhesion of microstructures [24,26]. Therefore, the sum of the van der Waals, capillary, and hydrogen bonding forces or surface disturbance forces in the microwire is predicted from the following relationship, in which the effect of covalent bonds, Casimir forces, asperity nano-welding, and dipole-dipole interactions, if any, is considered to be insignificant and negligible [24,26]. [24,26].

$$F_{Vand} + F_{Elec} + F_{Hydr} + F_{Capi} = F_{Adhe}$$

Where , $F_{Vand}, F_{Hydr},$ and F_{Capi} represent the van der Waals, hydrogen bonding, and capillary forces in the microstructure, respectively.

$$F_{Vand} + F_{Hydr} + F_{Capi} = F_{Adhe} - F_{Elec} = (0.118034 - 0.02014)\ \mu N = 0.097894\ \mu N$$

The sum of the three surface forces contributing to adhesion in the microwire is predicted to be 0.097894 μN. This study revealed that the external disturbance developed in the microwire from the different external fields/forces is 0.177 μN, which is higher than the adhesive force of 0.118 μN and 59.6 % of the total disturbance (0.297 μN). The external disturbances are developed due to the interaction of temperature, magnetic and electric fields, damping, and also force developed by the eddy current, Hall, and Seebeck effects. The proper function and reliability of the MEMS cannot be achieved without considering the effect of the external disturbance in microstructures. Besides, the sum of the van der Waals, capillary, and hydrogen bonding forces or surface disturbance forces in the microwire is 0.097894 μN, which is also dominant than the electrostatic force of 0.02014 μN and contributes adhesion in the microstructure. The electrostatic force causes structural and pull-in instability, unusual deformation, and effects dynamic attributes of microstructures [23]. The surface forces, such as capillary, hydrogen bonding, and van der Waals, cause adhesion and stiction and lead to dysfunction of MEMS [24,26]. Therefore, their quantification is essential for the appropriate design of MEMS devices. However, the

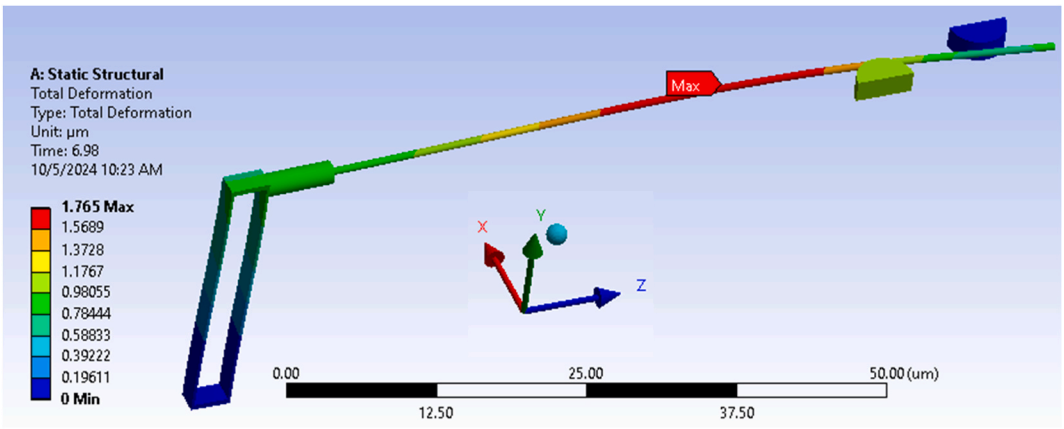

Fig. 10. Deformation of microwire with disturbance force 'F'.

direct measurement of surface and external disturbances is expensive and requires unique experimental setup and skills because of microscale size and tribology effects; in contrast, analytical prediction is also complex due to the nonlinearities, nonideal conditions, electro-mechanical coupling, and lack of suitable mathematical models [23,38]. This study explores a novel process of evaluating disturbances in the microstructure by synthesized experimental and numerical study and without using force sensors.

3.3. Validation

The deformation and contact behavior of the microwire are found to be consistent with the contact behavior without applying the total disturbance force 'F' at the free end of the microwire, which is presented in the study of Rahman and Akanda [1] and shown in Fig. 10. The maximum lateral deflection with disturbance force F = 0.295 μN is found to be 1.765 μm, whereas it is found 1.6063 μm [1] in without applying disturbance force. It indicates the appropriateness and accuracy of this study. Since the unusual deformation or out-of-plane bending is not observed in the microwire due to the applied force, 'F = 0.295 μN' at the free end, it is also supported by the column buckling analysis of the extended portion of the microwire.

The extended portion of microwire (5.0 μm) is subject to a maximum compressive force of 0.295 μN and supported at the 'Load Probe' by the resistive contact force. It is ensured that the applied force does not exceed the critical load of the fixed-free end column of length 5.0 μm.

$$\text{Microwire dia.}, d = 0.625\ \mu m, \text{Length}, L = 5.0\ \mu m, \text{End condition}, C = \frac{1}{4}\ (\text{fixed} - \text{free})$$

$$\text{Radius of gyration}, \rho = \sqrt{\frac{I}{A}} = 1.563 \times 10^{-7}\ \text{m}, \text{Slenderness ratio}, \left(\frac{L}{\rho}\right) = 32$$

$$\text{Yied strength}, \sigma_y = 630\ MPa, \quad \text{Modulus of elasticity}, E = 1.76 \times 10^5\ MPa \quad [11,\ 23]$$

Critical slenderness ratio, $\left(\frac{L}{\rho}\right)_{cr} = \sqrt{\frac{2\pi^2 E C}{\sigma_y}} = 37$ and $\left(\frac{L}{\rho}\right) < \left(\frac{L}{\rho}\right)_{cr}$. Johnson equation of column [50], $P_{cr} = A\left[\sigma_y - \left(\frac{\sigma_y}{2\pi}\frac{L}{\rho}\right)^2 \frac{1}{CE}\right] = 122\ \mu N.$

The force applied at the free end of the microwire is much less than the critical buckling load of 122 μN. Therefore, unusual deformation is not observed in the extended portion of the microwire, which also supports the appropriateness of this study.

The stick and slip motions of the microwire during pushing forward and pulling backwards are also compared with the available experimental study [11] for validation of the numerical analysis. The intensity of stick and slip motion is found less in the numerical analysis than in the experimental study, as shown in Fig. 11(a–d). It happened since the numerical investigation was accomplished without the presence of any disturbance force. However, the experimental study is done in the presence of all disturbance forces. It revealed the appropriateness and validity of the numerical analysis.

4. Conclusions

The disturbance forces in microstructures play crucial roles in the functionality, trustworthiness, and endurance of MEMS sensors and devices. They are used to monitor brain activity, respiratory organs, developing drugs, blood vessels, vital sign detection, robotic surgery, and other crucial fields, such as automobiles, defenses, communication, GPS, etc. Besides, some microstructures, such as micro-cantilevers, are used to manipulate micro-objects, biological cells, tissues, and embryos in medical research. Therefore, quantification of disturbances in microstructures is vital. In this study, the total amount of disturbance, including the surface and external disturbance in a platinum microwire, is quantified through the synthesized experimental and numerically predicted contact force. The sum of total disturbances in the platinum microwire is predicted to be 0.295 μN, which includes disturbances from surface forces and also forces arising from external sources or fields. The disturbance from external fields or sources is quantified to be 0.177 μN and from surface or adhesive force is 0.118034 μN. The electrostatic force is assessed to be 0.02014 μN. Also, the sum of van der Waals, capillary, and hydrogen bonding is predicted to be 0.097894 μN. This study also revealed that, besides adhesive force, the force arising from external fields or sources has a significant effect on the contact and mechanical behavior of microstructures. Its effects cannot be ignored during the evaluation of the mechanical behavior of microstructures and the design of MEMS sensors and devices. In this study, disturbance forces in the microwire are quantified without using force sensors and costly experimental setups. The method presented in this study can be employed to quantify disturbance forces in different microstructures, such as microbars, microplates, microrods, etc., and also evaluate the effects of disturbance forces on micro-contact behavior. Ultimately, it will aid in assessing the functionality, dependability, and endurance of MEMS sensors and microstructures more precisely and in reliable manipulation of micro-objects, such as biological cells, tissues, embryos, etc. Furthermore, this study opens the scope of investigating the effects of temperature, size, shape, and material on the contact behavior, friction, and disturbance force of the microstructure.

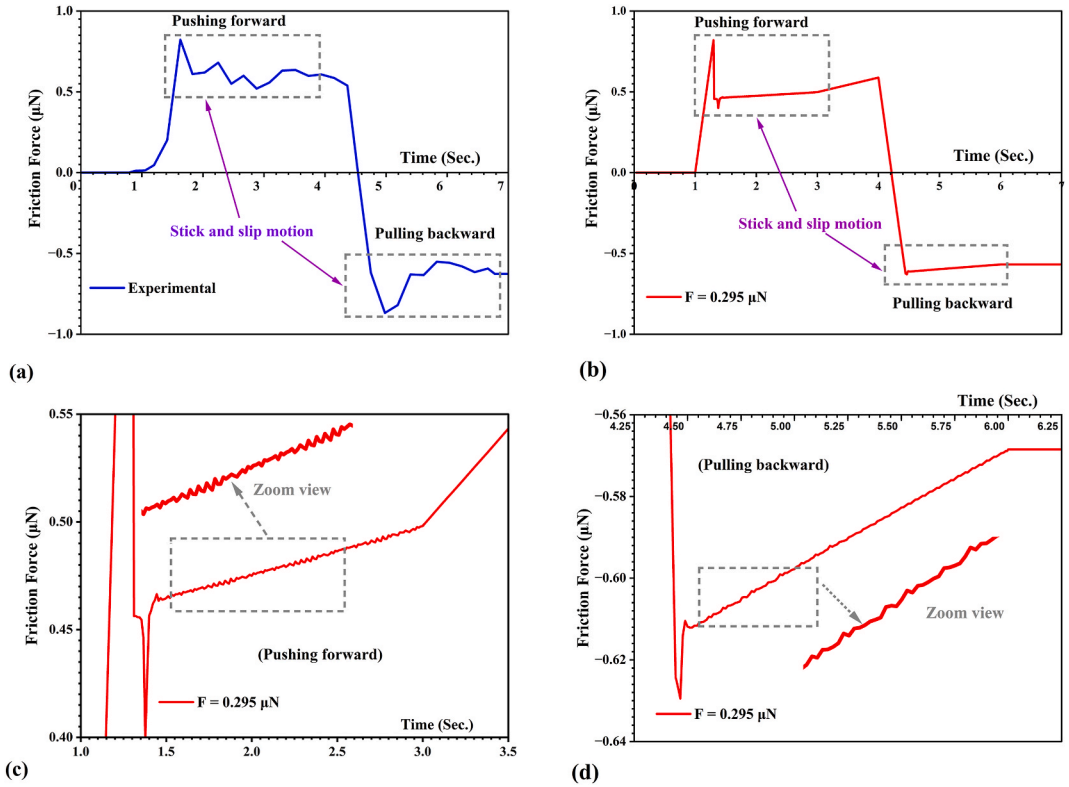

Fig. 11. Stick and slip sliding motion of microwire in (a) Experimental study, (b) Numerical analysis, (c) Magnified view of stick and slip motion during pushing forward, and (d) During pulling backward in numerical analysis.

CRediT authorship contribution statement

Fazlar Rahman: Writing – original draft, Methodology, Conceptualization. **M.A. Salam Akanda:** Writing – review & editing, Visualization, Validation, Supervision, Project administration, Methodology.

Data availability

Data of this study is available on request.

Declaration of competing interest

The authors declare that they have no known competing financial interests or personal relationships that could have appeared to influence the work reported in this paper.

Acknowledgement

The authors acknowledge the Bangladesh University of Engineering and Technology (BUET), Dhaka, Bangladesh, for facilitating this study, and the Department of Mechanical and Production Engineering (MPE) of Ahsanullah University of Science and Technology (AUST), Dhaka, for supporting the computational facility.

Nomenclature:

[K]	Global stiffness matrix
MEMS	Micro Electro-Mechanical Systems
{U}	Displacement vector
{F}	Input force vector
S	Stress stiffening matrix
S'	Spin softening matrix
V	Velocity

F_D	Total disturbance force
F_{Elec}	Electrostatic force
F_{Adhe}	Adhesive force
F_{E_distb}	External disturbance
F_{Vand}	van der Waals
F_{Hydr}	Hydrogen bonding
F_{Capi}	Capillary force
P_{cr}	Critical load of column
A	Cross section of microwire
DBC	Double Beam Cantilever
k	Stiffness of DBC
P_{cr}	Critical load in column

References

[1] F. Rahman, M.A.S. Akanda, Numerical analysis of reaction forces at the supports of sliding microwire, J. Mech. Eng. Sci. 14 (4) (2020) 7434–7445, https://doi.org/10.15282/jmes.14.4.2020.12.0586.

[2] M. Shikida, Y. Hasegawa, M.S. Al Farisi, M. Matsushima, T. Kawabe, Advancements in MEMS technology for medical applications: microneedles and miniaturized sensors, Jpn. J. Appl. Phys. 61 (SA) (2022) 803, https://doi.org/10.35848/1347-4065/ac305d.

[3] K.J. Rebello, Applications of MEMS in surgery, Proc. IEEE 92 (1) (2004) 43–55, https://doi.org/10.1109/JPROC.2003.820536.

[4] R. Ahmadi, M. Kalantari, M. Packirisamy, J. Dargahi, Modeling and optimal design of an optical MEMS tactile sensor for use in robotically assisted surgery, Photonics North 7750 (2010) 775008, https://doi.org/10.1117/12.872025, 2010.

[5] F. Rahman, M.A.S. Akanda, Mechanical and dynamic characteristics of double and single beam cantilevers for MEMS manipulation, J. Mech. Sci. Technol. 36 (9) (2022) 4635–4647, https://doi.org/10.1007/s12206-022-0825-z.

[6] L.A. Al-Haddad, A.A. Jaber, S.A. Al-Haddad, Y.M. Al-Muslim, Fault diagnosis of actuator damage in UAVs using embedded recorded data and stacked machine learning models, J. Supercomput. 80 (3) (2024) 3005–3024, https://doi.org/10.1007/s11227-023-05584-7.

[7] T. Gao, W. Sheng, M. Zhou, B. Fang, L. Zheng, MEMS inertial sensor fault diagnosis using a CNN-based data-driven method, Int. J. Pattern Recogn. Artif. Intell. 34 (14) (2020) 2059048, https://doi.org/10.1142/S021800142059048X.

[8] M. Pustan, S. Paquay, V. Rochus, J.C. Golinval, Modeling and finite element analysis of mechanical behavior of flexible MEMS components, Microsyst. Technol. 17 (2011) 553–562, https://doi.org/10.1007/s00542-011-1232-z.

[9] T.W. Lin, A. Modafe, B. Shapiro, R. Ghodssi, Characterization of dynamic friction in MEMS-based microball bearings, IEEE Trans. Instrum. Meas. 53 (3) (2004) 839–846, https://doi.org/10.1109/TIM.2004.827089.

[10] J.K. Sakellaris, Finite element analysis of micro-electro-mechanical systems: towards the integration of MEMS in design and robust optimal control schemes of smart microstructures, WSEAS Trans. Appl. Theor. Mech. 3 (4) (2008) 114–124.

[11] M.A. Salam Akanda, H. Tohmyoh, M. Saka, Precision friction measurement between ultrathin wire and microprobe, Sensor. Actuator. 172 (1) (2011) 189–194, https://doi.org/10.1016/j.sna.2011.05.020.

[12] Q.-S. Bai, K. Cheng, B. He, Y.C. Liang, Design of a novel tensile testing device and its application in tensile testing experiments on copper micro wires, Proc. IME B J. Eng. Manufact. 226 (9) (2012) 1594–1600, https://doi.org/10.1177/0954405412454058.

[13] L. Lai, G. Yu, G. Wang, Y. Li, G. Ding, Z. Yang, Application of Ni/SiCw composite material in MEMS microspring, Micromachines 14 (9) (2023) 1767, https://doi.org/10.3390/mi14091767.

[14] MEMSNet, What is MEMS Technology, Available online: https://www.memsnet.org/mems/what_is.html, 2022.

[15] N. Tayebi, A.A. Polycarpou, Reducing the effects of adhesion and friction in microelectromechanical systems (MEMSs) through surface roughening: comparison between theory and experiments, J. Appl. Phys. 98 (7) (2005) 073528, https://doi.org/10.1063/1.2058178.

[16] N. Kilinc, O. Cakmak, A. Kosemen, E. Ermek, S. Ozturk, Y. Yerli, Z.Z. Ozturk, H. Urey, Fabrication of 1D ZnO nanostructures on MEMS cantilever for VOC sensor application, Sensor. Actuator. B Chem. 202 (2014) 357–364, https://doi.org/10.1016/j.snb.2014.05.078.

[17] T.E. Buchheit, B.L. Boyce, G.W. Wellman, The role of microstructure in MEMS deformation and failure, ASME International Mechanical Engineering Congress and Exposition 36428 (2002) 559–566.

[18] K. Komvopoulos, Adhesion and friction forces in microelectromechanical systems: mechanisms, measurement, surface modification techniques, and adhesion theory, J. Adhes. Sci. Technol. 17 (4) (2003) 477–517, https://doi.org/10.1163/15685610360554384.

[19] F. Yang, J.C. Li, Micro and Nano Mechanical Testing of Materials and Devices, Springer, 2008, https://doi.org/10.1007/978-0-387-78701-5.

[20] J. Biener, A. V Hamza, A.M. Hodge, Deformation behavior of nanoporous metals, in: Micro and Nano Mechanical Testing of Materials and Devices, Springer, 2008, pp. 118–135.

[21] A.K. Waghmare, P. Sahoo, Adhesive friction at the contact between rough surfaces using n-point asperity model, Engineering Science and Technology, an International Journal 18 (3) (2015) 463–474, https://doi.org/10.1016/j.jestch.2015.03.006.

[22] R. Maboudian, C. Carraro, Surface chemistry and tribology of MEMS, Annu. Rev. Phys. Chem. 55 (2004) 35–54, https://doi.org/10.1146/annurev.physchem.55.091602.094445.

[23] F. Rahman, M.A.S. Akanda, Quantification of electrostatic and adhesive forces between microwire and microprobe using experimental and numerical approaches, Arabian J. Sci. Eng. 49 (2) (2024) 1673–1682, https://doi.org/10.1007/s13369-023-07977-5.

[24] A. Basu, G.G. Adams, N.E. McGruer, A review of micro-contact physics, materials, and failure mechanisms in direct-contact RF MEMS switches, J. Micromech. Microeng. 26 (10) (2016) 104004, https://doi.org/10.1088/0960-1317/26/10/104004.

[25] M. Tausiff, H.M. Ouakad, H. Alqahtani, Global nonlinear dynamics of MEMS arches actuated by fringing-field electrostatic field, Arabian J. Sci. Eng. 45 (7) (2020) 5959–5975, https://doi.org/10.1007/s13369-020-04588-2.

[26] N. Tas, T. Sonnenberg, H. Jansen, R. Legtenberg, M. Elwenspoek, Stiction in surface micromachining, J. Micromech. Microeng. 6 (4) (1996) 385–397, https://doi.org/10.1088/0960-1317/26/10/104004.

[27] Z. Yapu, Stiction and anti-stiction in MEMS and NEMS, Acta Mech. Sin. 19 (1) (2003) 1–10, https://doi.org/10.1007/bf02487448.

[28] G. Biresaw, K.L. Mittal, Surfactants in Tribology, CRC Press, Boca Raton, 2008.

[29] A.L. Herrera-May, J.C. Soler-Balcazar, H. Vázquez-Leal, J. Martínez-Castillo, M.O. Vigueras-Zuñiga, L.A. Aguilera-Cortés, Recent advances of MEMS resonators for Lorentz force based magnetic field sensors: design, applications and challenges, Sensors 16 (9) (2016) 1359, https://doi.org/10.3390/s16091359.

[30] A. Somà, A survey of Mechanical failure and design for Reliability of MEMS, in: IOP Conference Series: Materials Science and Engineering, vol. 724, IOP Publishing, 2020 12051, https://doi.org/10.1088/1757-899X/724/1/012051.

[31] D. Fu, A.X. Levander, R. Zhang, J.W. Ager, J. Wu, Electrothermally driven current vortices in inhomogeneous bipolar semiconductors, Phys. Rev. B 84 (4) (2011) 045205, https://doi.org/10.1103/PhysRevB.84.045205.

[32] F. Rahman, M.A.S. Akanda, Minimizing surface driving and disturbance forces in MEMS's microstructure-A review, Ann. Eng. 2 (1) (2021) 1–17.
[33] S.R. Das, Focus : temperature difference leads to magnetism, Am. Phys. Soc. (APS). 28 (2) (2011).
[34] T.R. Hsu, Reliability in MEMS packaging, in: IEEE International Reliability Physics Symposium Proceedings, 2006, pp. 398–402, https://doi.org/10.1109/RELPHY.2006.251251.
[35] R. Maboudian, C. Carraro, Surface engineering for reliable operation of MEMS devices, J. Adhes. Sci. Technol. 17 (4) (2003) 583–591, https://doi.org/10.1163/15685610360554429.
[36] D.J. Fonseca, M. Sequera, On MEMS reliability and failure mechanisms. Statistics, and Reliability, International Journal of Quality, 2011, p. 2011, https://doi.org/10.1155/2011/820243.
[37] J.A. Walraven, Future challenges for MEMS failure analysis, IEEE International Test Conference (TC) (2003) 850–855, https://doi.org/10.1109/test.2003.1271070.
[38] W.C. Chuang, H.L. Lee, P.Z. Chang, Y.C. Hu, Review on the modeling of electrostatic MEMS, Sensors 10 (6) (2010) 6149–6171, https://doi.org/10.3390/s100606149.
[39] M. Shavezipur, G.H. Li, I. Laboriante, W.J. Gou, C. Carraro, R. Maboudian, A finite element technique for accurate determination of interfacial adhesion force in MEMS using electrostatic actuation, J. Micromech. Microeng. 21 (11) (2011) 115025, https://doi.org/10.1088/0960-1317/21/11/115025.
[40] M.P. De Boer, T.M. Mayer, Tribology of MEMS, MRS Bull. 26 (4) (2001) 302–304.
[41] C. Deng, Y. Mao, G. Ren, MEMS inertial sensors-based multi-loop control enhanced by disturbance observation and compensation for fast steering mirror system, Sensors 16 (11) (2016) 1920, https://doi.org/10.3390/s16111920.
[42] L. Dong, J. Edwards, Active disturbance rejection control for an electro-statically actuated MEMS device, International Journal of Intelligenct Control and Systems 16 (3) (2011) 160–169.
[43] S. Liu, A. Davidson, Q. Lin, Simulation studies on nonlinear dynamics and chaos in a MEMS cantilever control system, J. Micromech. Microeng. 14 (7) (2004) 1064–1073, https://doi.org/10.1088/0960-1317/14/7/029.
[44] Q. Zheng, L. Dong, D.H. Lee, Z. Gao, Active disturbance rejection control for MEMS gyroscopes, IEEE Trans. Control Syst. Technol. 17 (6) (2009) 1432–1438, https://doi.org/10.1109/TCST.2008.2008638.
[45] Y. Qiao, W. Xu, J. Sun, H. Zhang, Reliability of electrostatically actuated MEMS resonators to random mass disturbance, Mech. Syst. Signal Process. 121 (2019) 711–724, https://doi.org/10.1016/j.ymssp.2018.11.055.
[46] F. Rahman, M.A.S. Akanda, Measurement and controlling friction force in a sliding microwire by size and boundary condition variation, Proceedings of ICME 14th Internatoinal Conference on Mechanical Engineering 18–19 (2023) 1–7, 311.
[47] P.R. Barrett, ANSYS nonlinear convergence best practices, CAE Assoc (2016).
[48] Contact Technology Guide Release 12.1, ANSYS Inc., 2009.
[49] H.-H. Lee, Finite Element Simulations with ANSYS Workbench, SDC Publications, 2019.
[50] R.G. Budynas, J.K. Nisbett, Shigley's Mechanical Engineering Design, tenth ed., McGrawHill, New York, 2015.